

Keywords

Global Heat Flow,
Digital Maps,
GIS Techniques,

Received: January 28, 2018

Accepted: April 18, 2018

Published: April 26, 2018

Global Heat Flow: New Estimates Using Digital Maps and GIS Techniques

Fábio Vieira¹, Valiya Hamza¹

¹Observatório Nacional, Rio de Janeiro, Brazil.

Email address

valiyahamza@gmail.com (V. Hamza)

Corresponding author

Abstract

The digital geophysical maps and GIS (Geographic Information System) techniques have been employed in obtaining a better understanding of global heat flow. The starting point has been a system of 1° x 1° equal longitude grid consisting of 64800 cells. Superposed on this grid system are a set of 190 polygons that approximates boundaries of tectonic provinces and another set of 137 polygons that outlines age provinces. The area extents of these “tectonic polygons” were determined, and heat flow values calculated based on the empirical relation between heat flow and age of last thermos-tectonic event. Maps derived using such polygon representations reveal a pattern quite similar to that obtained in higher-degree spherical harmonic representations of global heat flow. In addition, an updated assessment of observational data has been carried out and estimated values assigned for cells where observational data are currently unavailable. This practice has been found to provide reasonable bounds in interpolations, leading to better representations of heat flow on a global scale. The mean global heat flow values obtained by this procedure is found to fall in the interval of 58 to 63mW/m². This estimate is lower than that reported in some of the previous studies in which use has been made of theoretical values derived from half-space cooling models as substitutes for experimental data. According to the results of the present work, based on reappraisal of global heat flow database and with due emphasis on observational data, the global conductive heat loss falls in the range of 28 to 35TW. This is nearly 22 to 35% less than those reported in earlier studies.

1. Introduction

Measurements of terrestrial heat flow in boreholes penetrating the near surface layers provide valuable information on the internal thermal field of the Earth and estimates of global heat loss. The problem however is that availability of experimental data is not available for all regions, there being large areas without suitable data. One of the ways of getting around this problem is to employ empirical relations between heat flow and geological characteristics of near surface layers. Preliminary indications of a correlation between heat flow and geologic age was pointed out by Hamza (1967). Following this, empirical relations between heat flow and tectonic age were proposed (Polyak and Smirnov, 1968; Hamza and Verma, 1969). In a later work (Chapman and Pollack, 1975) derived maps of global heat flow where the empirical relation with age was employed in estimating heat flow values for areas for which experimental data were not available. In the procedure adopted by Chapman and Pollack (1975) the heat flow estimates were made on the basis of dominant geological features identifiable in 5° x 5° equal longitude cells. A similar procedure was adopted by Pollack et al (1993) in deriving improved global heat flow maps

where the referencing system for tectonic age was based on a grid of 1° x 1° equal longitude cells. However, selection of dominant geology in each cell and estimation of number of cells were manual and prone to potential errors. More importantly, Pollack et al (1993) employed theoretical heat flow values, derived from half-space cooling model, as substitutes of observational data for regions of oceanic crust with ages less than 55 Ma. Validity of this approach was questioned by Hamza et al (2008a). In the later works of Davies and Davies (2010) and Vieira et al (2010) it was pointed out that the adverse effects of some of these problems may be minimized by adopting the use of modern techniques of handling geospatial data.

Techniques developed in Geographic Information System (GIS) are particularly suitable for elaboration of digital geological and geophysical maps and in handling irregularly spaced data sets. Clearly, polygons may be employed in outlining boundaries of tectonic units. A major advantage of GIS techniques is in matching areas of heat flow measurements with “tectonic” polygons and in estimating errors with appropriate weighting by area. However, the empirical relation used by Davies and Davies (2010) makes use of theoretical values derived from half-space cooling

model for ocean regions with ages less than 55 Ma. In the present work, it is argued that values derived from half-space cooling models lead to overestimation heat flow for young ocean crust.

2. Digital Maps and GIS Techniques

Availability of digital thematic maps based on techniques of geographic information system (GIS) has opened up the possibility of assigning theoretical heat flow values, with improved accuracy. This technique also allows appropriate weighting for the tectonic context and is particularly suitable for elaboration of digital geological and geophysical maps and in handling irregularly spaced data sets. The digital maps of 1° x 1° cells for continental and oceanic regions, adapted from Mooney et al (1998) and Muller et al (1997), are illustrated in Figure 1.

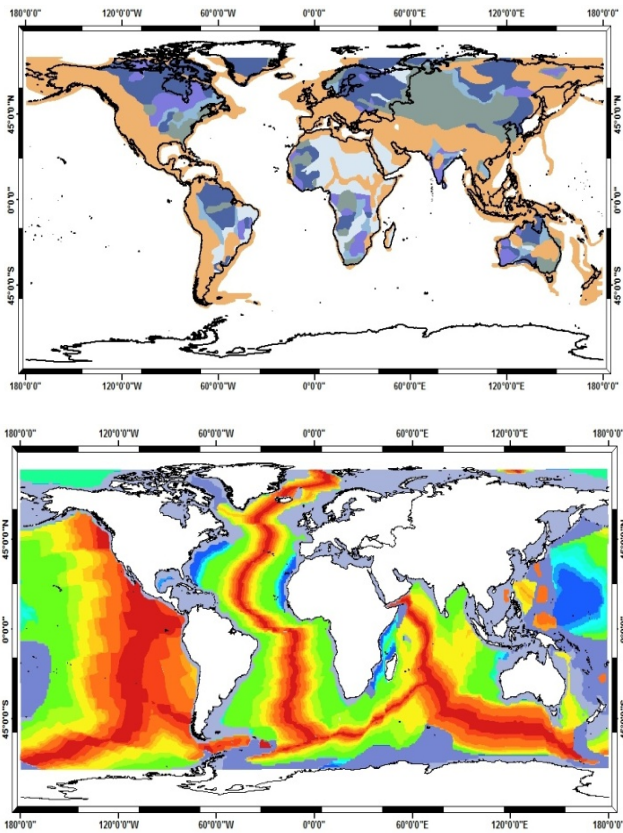


Figure 1 - Digital maps of tectonic units employed in obtaining estimates of terrestrial heat flow. The top panel refers to digital map of tectonic provinces in continental regions. The bottom panel refers to digital isochrone map for oceanic regions (Adapted from Hamza and Vieira, 2010).

Global geophysical maps of tectonic provinces presented by Mooney et al (1998) cover platforms, shields, large igneous provinces, basins, orogens and areas of extended crust. Also provided in this reference are global maps of last tectonic events for the geologic periods of Arquean, Proterozoic (early, middle and late periods), Paleozoic and Meso-Cenozoic. Digital isochrone maps by Muller et al (1997) allow identification of age provinces in oceanic regions. In the present work, we make use of digitized versions of these maps in investigating the nature of terrestrial heat flow variations on global scale.

In the work of Vieira et al (2010) the procedure adopted in handling digital maps consists of outlining tectonic units over 1° x 1° equal longitude grids. Such a grid system consists of 64800 cells. Of these 22.380 cells cover the continental crust and 42.420 cells cover the oceanic crust. The changes relative to the data set reported by Vieira et al (2010) include incorporation of improved data sets for the South American continent. In particular, there has been significant improvement in the number of heat flow values in Colombia (reported in INGEOMINAS, 2009) and recent new data for central and northern regions (Vieira, 2010) of Brazil.

According to the updated data sets 44386 grid elements have one or more observational data. Estimated heat flow values were employed for the remaining 54769 grid elements. Six categories of tectonic age were used in outlining the polygons. A set of 137 polygons was found sufficient in delimiting the tectonic age pattern for continental areas. In the case oceanic areas 15 categories of tectonic age were used in outlining the polygons. A set of 13 polygons was found sufficient in delimiting the tectonic age pattern. Superposed on this grid system are a set of 190 polygons that delimit the boundaries of tectonic provinces and another set of 137 polygons that delimit the tectonic age pattern.

3. Estimates of Heat Flow for Polygons

Following the practice adopted by Mooney et al (1998) the tectonic age provinces considered in calculations of estimated heat flow values in continental areas are Arquean, Paleo Proterozoic, Meso-Proterozoic, Neo-Proterozoic, Paleozoic and Meso-Cenozoic. Updated data sets were employed in calculating mean values of heat flow for these provinces lying in the continents of North America, South America, Europe, Africa, Asia and Australia. Table 1 provides a summary of the results obtained. It reveals a general trend of decreasing heat flow with age. Thus, relatively high heat flow values were found for younger provinces of Cenozoic and Mesozoic ages, compared with those of older ones with Proterozoic and Arquean ages. For example, heat flow in excess of 80mW/m² occur in all continental age provinces of Meso-Cenozoic times. On the other hand, all Arquean shields have heat flow less than 50mW/m².

Table 1 - Summary of mean heat flow values assigned for tectonic polygons in continental regions. The abbreviations used are: NA – North America; SA – south America; EU – Europe; AF – Africa; AS – Asia; AU – Australia.

Tectonic Age	Heat Flow (mW/m ²)					
	NA	SA	EU	AF	AS	AU
Cenozoic	120	81	78	82	88	100
Mesozoic	75	64	72	81	63	80
Paleozoic	52	46	47	64	54	79
Neo Proterozoic	48	74	43	65	63	83
Paleo Proterozoic	46	64	44	53	59	61
Arquean Shields	50	45	42	49	46	40

In the case of oceanic regions thirteen different age categories were considered, following the classification scheme of Muller et al (1997). Table 2 provides a list of mean heat flow values reported by Pollack et al (1993), for areas delimited on the basis of ocean floor isochrones. Here also the

general a general trend of decreasing heat flow with age of ocean floor is observed. Thus, heat flow in excess of 80mW/m² are found in young ocean crust with ages less than 20Ma.

Table 2 - Summary of mean heat flow values assigned for tectonic polygons in oceanic regions (adapted from Pollack et al, 1993).

Age Interval (Ma)		Heat Flow (mW/m ²)
Lower	Upper	
0	11	132
11	20	88
20	33	74
33	40	66
40	48	63
48	68	58
68	83	54
83	127	49
127	132	47
132	140	46
140	148	45
148	154	45
154	180	44

In determining heat flow variations on the basis of polygons of age provinces it is convenient to make use of an equation that accounts for the nature of the empirical relation. In the present context, a relation that allows for variation of heat flow with inverse square root of age seems appropriate. Such an equation may be written as:

$$q(t) = c * \left(\frac{\alpha}{\sqrt{t}} + \beta \right) \quad (1)$$

where q(t) is the heat flux at time t, c is a scaling constant and α and β are terms employed in numerical approximation. The parameter α is related to the “degree of influence” of thermo-tectonic event on the crustal layers. Thus, the product C*α has an inverse relation with heat flow. The parameter β may be considered as representative of heat flow in old crust, where thermal contributions of older tectonic events are relatively insignificant at present times. The variation of heat flow with age for continental regions, derived from data reported in Polyak and Smirnov (1968), Hamza and Verma (1969) and Pollack et al (1993), is illustrated in Figure 2.

In this figure the left panel illustrates the variation heat flow with the inverse square root of age. The right panel indicates variation heat flow as a function of age for three different values of the product c*α. The fit indicated by the blue curve has the value of 422 for the product C*α. This value is in reasonable agreement with that proposed by Hamza (1979). The red and black curves may be considered as indicative of upper and lower bounds that bracket the observational trends. A summary of the parameters employed the fits is provided in Table 3.

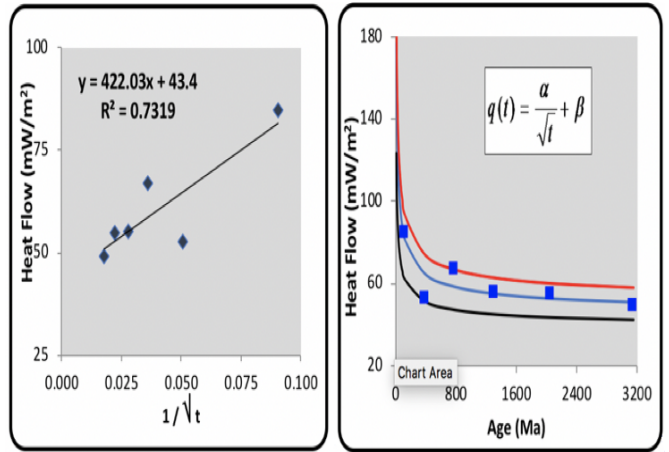


Figure 2 - Relations between heat flow (q) and age (t) for continental regions (left and right panels). The red and black curves indicate upper and lower bounds.

Table 3 - Parameters of equation 1 for continental regions.

FIT	C	α	β
Mean	1	422	43
Upper Bound	1.4	350	35
Lower Bound	0.9	300	42

The variation of heat flow with age for oceanic regions is illustrated in Figure 3. As in the case of continental regions discussed above, the left panel illustrates the variation heat flow with the inverse square root of age while the right panel indicates variation heat flow as a function of age for three different values of the product c*α. The fit is indicated by the blue curve refer to a value of 120 for the product C*α. The red curve, for which the value of the product C*α is 192, may be considered as the upper bound. The black curve for which the value of the product C*α is 72 may be considered as the lower bound. A summary of the parameters employed in such fits is provided in Table 4.

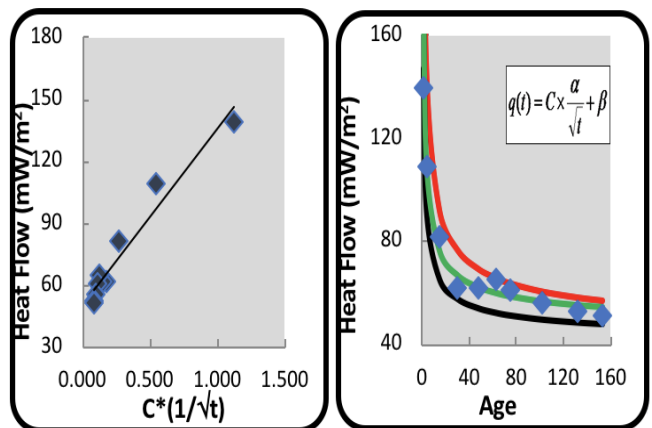


Figure 3 - Relations between heat flow (q) and age (t) for oceanic regions (left and right panels). The red and black curves indicate upper and lower bounds.

Table 4 - Parameters of equation -1 for oceanic regions.

FIT	C	α	β
Selected	1	120	45
Upper Bound	1.2	160	35
Lower Bound	0.8	90	35

3. Global Map of Cell-Averaged Values

The map of global heat flow derived on the basis of cell-averaged values, with weighting for the tectonic context, is illustrated in Figure 4. Note that assigning cell averaged values of heat flow for the tectonic polygons have led to considerable improvements in outlining boundaries of associated heat flow anomalies Vieira and Hamza (2011). For example, most of the regions with high heat flow anomalies (with values higher than 60mW/m²) are associated with lithospheric plate boundaries, while most of the ocean basins and interior parts of continental regions are characterized by heat flow less than 60mW/m². Also, the widths of high heat flow anomalies associated with mid-ocean ridge areas are narrower.

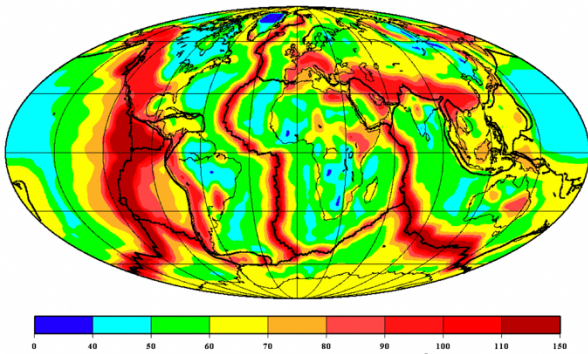


Figure 4 - Global representation of estimated heat flow values (in units of mW/m²), based on digital maps and empirical relation with age (Modified after Vieira and Hamza, 2011; Hamza, 2013).

5. Global map of Observational Data

The global heat flow database in its present form is an outgrowth of earlier compilations (e.g. Birch, 1954; Lee, 1963; Lee and Uyeda, 1965; Jessop et al, 1976; Chapman and Pollack, 1975; Pollack et al, 1993; Hamza et al, 2008a). In the present case, we have used an updated data set of surface heat flow that includes information available in the original compilation of the International Heat Flow Commission - IHFC, additional values reported in the recent study of Davies and Davies (2010) as well as updated values for the South American continent (Vieira and Hamza, 2011). In the earlier works (Pollack et al, 1993; Davies and Davies, 2010) heat flow values assigned to cells located in areas of young ocean crust have been derived on the basis of the half-space cooling – HSC model of Stein and Stein (1992). In later works Vieira and Hamza (2011), Hamza (2013) and Cardoso and Hamza (2011) use was made of values derived from the Finite Half-Space – FHS model. A summary of data sets, employed in deriving global heat flow maps is provided in Table 5.

The total number of heat flow values in the updated data set is 44386. The locations of heat flow measurements of the updated data sets are illustrated in the map of Figure 5.

Note that there are significant variations in data density. Antarctica, Greenland and central parts of Africa and South America remain as regions of low data density. This data set has been employed in calculating mean values for a global grid system composed of 1° x 1° equal longitude cells. In spite of recent advances in in experimental works the number of cells for which observational data are unavailable is nearly 20%. This poses a serious problem in deriving global maps based exclusively on observational data. In such cases, it is clear that

some type of interpolation scheme is necessary in assigning “representative” values to empty cells.

Table 5 - Summary of data sets employed in deriving global heat flow maps. N refer to number of Observational data.

Reference	N	Cell size	Values for Young Ocean Crust
4	20201	5° x 5°	Observational data
5	20201	5° x 5°	Half-space cooling model - HSC
6	24141	2° x 2°	Observational data
7	38374	Variable; polygons	Half-space cooling model - HSC
13, 14, 20	43049	Variable; Polygons	Data and Finite Half-Space model - FHS

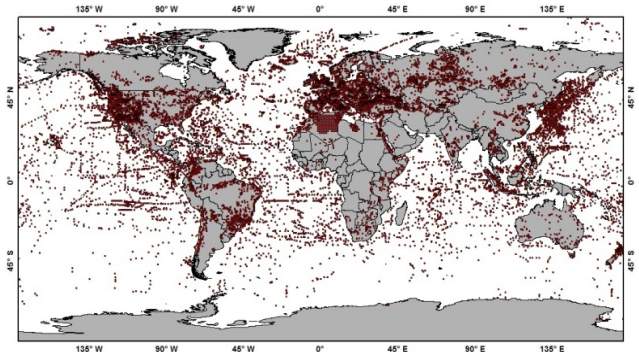


Figure 5 - Locations of heat flow measurements as per the updated global heat flow data set (Modified after Vieira and Hamza, 2011; Hamza, 2013).

It is convenient to note in this context that the availability of estimated heat flow with appropriate weighting for the tectonic setting has opened up the possibility of assigning representative values of heat flow for cells for which observational data are currently not available. This in practice amounts to use of a mixed data set consisting mostly of bin averaged values derived from observational data along with a small set of suitably selected estimated values. A geographic distribution of integrated data sets (observational data and estimated values) is illustrated in figure 6. Here a 5° x 5° mesh system was used for a representation of the data sets. In this figure cells with the experimental data are indicated in red color and cells with estimated heat flow values in white.

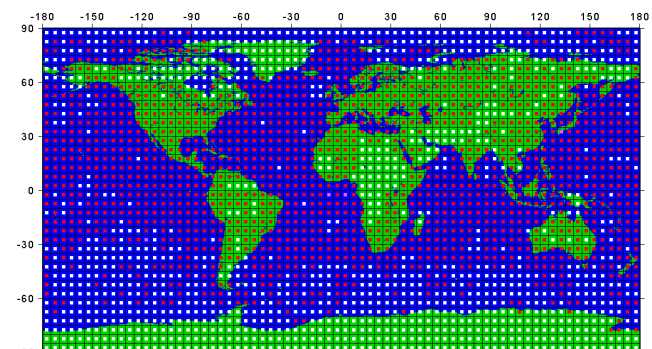


Figure 6 - Illustration of cell averaged data distribution based on a 50x50 mesh system. The background color for continental areas is green and that for oceanic areas blue.

It must however be noted that heat flow values assigned to cells located in areas of young ocean crust have been derived on the basis of FHS model. The cell-averaged heat flow values are in the range of 30 - 150 mW/m². The mean heat flow for cells in the continental regions is 58 +/- 10 mW/m², which is not significantly different from that for cells in the oceanic regions. The global heat flow map derived on the basis of such a mixed data set is presented in Figure 7.

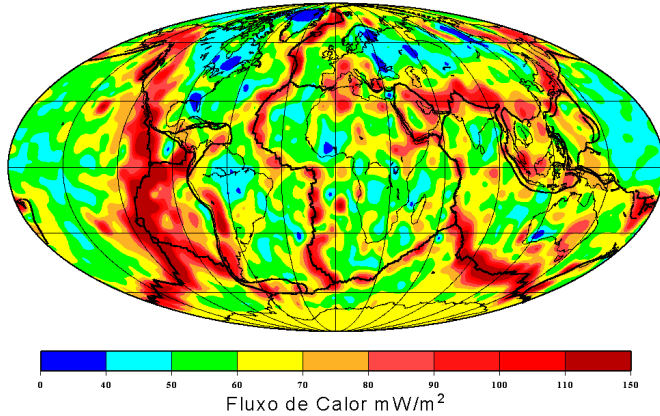


Figure 7 - Global representation of heat flow based on observational data, supplemented with estimates derived from digital maps and empirical correlation with age (Modified after Vieira and Hamza, 2011; Hamza, 2013).

It is readily apparent that the large-scale features present in this map are quite similar to those of the theoretical heat flow map of Figure 5. Thus, the divergent plate boundary regions (such as the Nazca plate in the Pacific, areas off the west coast of the United States, the Sea of Japan and the Red Sea) stand out as oceanic regions of relatively high heat flow (>80 mW/m²). Also, mid-ocean ridges in the Atlantic, Pacific and Indian oceans also appear as areas of high heat flow (typically in the range 90-150 mW/m²). The ocean basins and areas of low angle subduction appear to be characterized by normal heat flow (in the range 50-70 mW/m²). On the contrary, the central parts of the continental areas of Africa, Asia, North America, South America, Antarctica and Australia seem to be characterized by relatively low heat flow (<60 mW/m²).

6. Discussion

The discussion here is focused on the differences between heat flow maps of the present work and those of previous ones. As mentioned earlier, most of the differences originate from the use of model values employed in deriving estimates of heat flow values for young ocean crust. The previous works (Pollack et al, 1993; Davies and Davies, 2010) rely heavily on the use of half-space cooling (HSC) and Plate models in deriving estimated values. However, these models are known to be largely incompatible with observational data reported in Parsons and Sclater (1977) and Sclater et al (1980). A comparative analysis of the lithosphere models and procedures used in calculating heat flow values are provided in the following sections. This is followed a brief discussion of implications for global heat loss.

6.1. Lithosphere Model considerations

In the Half-Space Cooling (HSC) model the lithosphere is considered as the boundary layer of mantle convection cells.

The lithosphere grows in thickness continuously as it moves away from the up-welling limb of the mantle convection system. The cooling process of the lithosphere is assumed to be conductive and one-dimensional. The fit of HSC model curve to observational heat flow data is known to be poor (e.g. Hofmeister and Criss, 2005; 2006; 2008). It overestimates heat flow in ocean crust with ages less than 60 Ma and underestimates heat flow for crust with ages greater than 100 Ma (Parsons and Sclater, 1977; Sclater et al, 1980). Such difficulties arise from the implicit assumption of the HSC model that the wavelength of the problem domain is unbounded (Cardoso and Hamza, 2011). It implies that the thickness of the material undergoing solidification beneath the boundary layer is large compared to the stable thickness of the lithosphere at large distances from the ridge axis (Cardoso and Hamza, 2011). As pointed out by Hamza et al (2008) and Vieira et al (2010) this condition cannot be considered as satisfactory for the physical domain of the problem under consideration, since the upwelling material beneath the ridge axis has a finite width. Since this is the same magmatic material that moves laterally away from the ridge zone, its thickness has to be finite (Hamza, 2013).

The Plate model proposed by McKenzie (1967) is known to provide a better fit to heat flow data from ocean crust with ages greater than 100 Ma. Nevertheless, it also overestimates heat flow for ocean crust with ages less than 55 Ma. In an attempt to overcome such difficulties Stein and Stein (1992) proposed a hybrid version, referred to also as the Global Depth Heat Flow (GDH) reference model. The GDH model is successful in providing a satisfactory explanation for regional variations in bathymetry but fail in accounting for the low values of heat flow in ocean crust with ages less than 55 Ma. The problem eventually came to be known as the oceanic heat flow paradox. It was in this context that Stein and Stein (1992) and Pollack et al (1993) invoked the hypothesis of regional scale hydrothermal circulation in ocean crust as a possible mechanism responsible for the appearance of this paradox. Nevertheless, the proposed scheme of water circulation is based on the highly unreasonable assumption that lateral flow of cold water occurs over large distances through impermeable oceanic crust, from areas of stable segments away from spreading zones to areas near the ridge axis. Available evidences on hydrothermal circulation in ocean floor (see for example: Williams et al, 1974; Haymon et al, 1991; German et al, 1994) indicate that such processes are limited to narrow belts in the vicinity of spreading centers. There are no evidences for large scale subsurface flows in stable ocean crust. In addition, it seems unlikely that fluid pressure heads needed for driving such flows can be generated by differences in lateral temperatures.

It is clear that we need to look for alternatives that need not invoke the unlikely hypothesis of regional scale hydrothermal circulation in young ocean crust. Hamza et al (2010) considered the thermal consequences of variable rates of magma accretion at the lower boundary of the lithosphere. According to this model (designated Variable Basal Accretion - VBA) the variability in the rate of magma accretion at the base of the lithosphere has a direct influence on surface heat flux and bathymetry. More importantly, VBA has been found to be capable of accounting for the main features in observational data sets of heat flow and bathymetry, without the need to invoke the hypothesis of regional scale hydrothermal circulation in ocean crust. Nevertheless, VBA

does not address explicitly the thermal effects of latent heat at the lithosphere – asthenosphere boundary.

It was in this context that Cardoso and Hamza (2011) and Hamza (2013) proposed a new approach that incorporates the effects of latent heat and buffered solidification and at the same time provide a satisfactory solution for large scale variations of bathymetry and heat flux in the ocean floor. Designated as the Finite Half Space model - FHS, it introduces the assumption that the wavelength of the solution of the relevant heat conduction equation is related to the thickness of the stable lithosphere at large distances from the ridge axis. A major consequence of this assumption is that it imposes an asymptotic limit for the vertical growth of the lithosphere at the expense of the asthenosphere. Under these conditions the solution for the temperature (T) at depth (z) in the oceanic lithosphere of age (t) and of basal temperature (T_m) is (Cardoso and Hamza, 2011; Hamza, 2013):

$$T(z,t) = T_0 + (T_m - T_0) \frac{\text{erf}\left(\frac{z/2\sqrt{\kappa_{\text{mod}}t}}{a/2\sqrt{\kappa_{\text{mod}}t}}\right)}{\text{erf}\left(\frac{a/2\sqrt{\kappa_{\text{mod}}t}}{a/2\sqrt{\kappa_{\text{mod}}t}}\right)} \quad (2)$$

where *a* is the asymptotic value for the thickness of the lithosphere in stable ocean basins and *k_{mod}* is the modified thermal diffusivity, that takes into account the role of latent heat. A brief description of the theoretical basis of the FHS model and its application to heat flow is presented in the Appendix.

The relations for surface heat flux and bathymetry within the framework of the FHS model were also derived by Cardoso and Hamza (2011) and Hamza (2013). For the case of constant thermal diffusivity, the equation for surface heat flux in FHS model may be written as:

$$q(t)_{z=0} = \lambda \frac{(T_m - T_0)}{\sqrt{(\pi \kappa_{\text{mod}} t)}} \frac{1}{\text{erf}\left(\frac{a/2\sqrt{\kappa_{\text{mod}}t}}{a/2\sqrt{\kappa_{\text{mod}}t}}\right)} \quad (3)$$

A comparative illustration of the half-space and plate model fits is illustrated in figure 8. Note that FHS model provides a far better fit to experimental data than those found for other model fits.

A careful examination of Eq. (3) reveals that the solution provided by the FHS model represents the general case for thermal models of the lithosphere. In fact, it is possible to demonstrate that the solutions derived in the HSC and Plate models represent particular end member cases of the FHS model. Consider for example the solution (3) for small values of time and values of depth much less than the thickness of the stable lithosphere. In this case the right-hand side of Eq. (3) is nearly identical to that of the fundamental solution for temperature in the HSC model, the only difference being the modified form of thermal diffusivity. On the other hand, for depth values nearly equal to the stable thickness of the lithosphere the right-hand side of Eq. (1) approaches unity, which is the limiting condition employed in the Plate model of McKenzie (1967). In other words, the FHS model behavior is similar to that of the HSC model for small times but similar to that of the Plate model for large times.

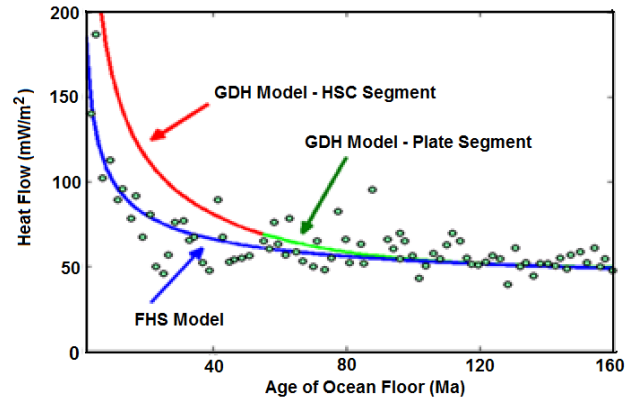


Figure 8 - Comparison of fits to observational oceanic heat flow data. Note that the fit for finite half-space model (FHS) is far superior when compared with those of HSC and GDH models (Adapted from Hamza, 2013).

6.2. Global Heat Loss

A topic of related interest is the problem of Global Heat Loss. Pollack et al (1993) reported a value of 44.2± 1.0 terawatt (TW) for global heat loss, which has found wide acceptance in the current literature. Similar estimates were also reported in the recent work of Davies and Davies (2010). In such estimates extensive use has been made of theoretical heat flow values, derived from the HSC model, in estimating heat losses for areas of young ocean crust. The justification for this practice (of using theoretical values as substitute for experimental data) is based on the argument that measured heat flow values in areas of young ocean crust are affected by the perturbing effects of hydrothermal circulation and hence not representative of total heat flux. However, the role of heat transport by hydrothermal circulation in young ocean crust and its influence on global heat loss has been examined in detail in a number of recent works (see for example: Hofmeister and Criss, 2005; 2006; 2008; Hamza et al, 2008b; Vieira et al, 2010). The main conclusion emerging from these studies is that hydrothermal circulation operates on local scales at or near the ridge axis. However, it is not an effective mechanism for heat transport on regional scales. In fact, as pointed out recently, the hypothesis of regional hydrothermal circulation (which assumes inflow of cold water in high heat flow areas and outflow of hot water in low heat flow areas) contradicts the very basic principles of thermal convection. According to the results of the present work, based on reappraisal of global heat flow database and with due emphasis on observational data, the global conductive heat loss falls in the range of 28 to 35TW. This is nearly 22 to 35% less than those reported in earlier studies.

7. Conclusions

In the present work digital geophysical maps and GIS techniques have been employed in delimiting spatial domains of tectonic provinces and age patterns and in obtaining better understanding of global heat flow. A system of 1° x 1° equal longitude grid consisting of 64800 cells was employed for this purpose. Superposed on this grid system are a set of 190 polygons that approximates boundaries of tectonic provinces and another set of 137 polygons that outlines age provinces. The area extents of these polygons were determined, and heat flow values calculated for this set of “tectonic polygons” based

on the empirical relation between heat flow and age of last thermos-tectonic event. Maps derived using such polygon representations reveal a pattern quite similar to those obtained in higher-degree spherical harmonic representations of global heat flow. In addition, an updated assessment of observational data has been carried out and estimated values assigned for cells for which observational data are currently unavailable. The mean global heat flow values obtained by this procedure is found to fall in the interval of 58 to 63mW/m².

The abovementioned range of values is lower than that reported in some of the previous studies in which use has been made of theoretical values derived from half-space cooling models as substitutes for experimental data. Finite half-space model is found to provide better estimates of heat flow for all age ranges of ocean crust, there being no need to invoke the hypothesis of regional hydrothermal circulation in ocean crust with ages greater than 20Ma.

According to the results of the present work, based on reappraisal of global heat flow database and with due emphasis on observational data, the global conductive heat loss falls in the range of 28 to 35TW. This is nearly 22 to 35% less than those reported in earlier studies.

8. Acknowledgment

This work was carried out as part of M.Sc. Thesis work of the first author. The second author is recipient of a research scholarship (Process No. 306755/2017-3) granted by Brazilian National Research Council - CNPq. We thank Dr. Papa for institutional support.

References

- Birch, F. 1954. The Present State of Geothermal Investigation, *Geophysics*, 19, 645-659.
- Cardoso, R.R., Hamza, V.M. (2011). Finite Half pace model of oceanic lithosphere. In: 'Horizons in Earth Science Research', Benjamin Veress and Jozsi Szigethy, (Editors), v.5, 151-162, ISBN 978161209X, Nova Science Publishers Incorporated.
- Cardoso, R.R., Ponte Neto, C.F.; Hamza, V.M. 2005. A reappraisal of global heat flow data. *Proceedings. 9th International Congress of the Brazilian Geophysical Society*. Salvador. Brazil. 6 pages.
- Chapman D.S., Pollack H.N. 1975. Global heat flow: a new look. *Earth Planet Sci Lett.*, 28, 23-32.
- Davies. J.H., Davies D.R. 2010. Earth's surface heat flux. *Solid Earth*. Vol. 1. p. 5-24.
- German, C.R., Briem, J., Chin, C., Danielsen, M., Holland, S., James, R., Jonsdottir, A, Ludford, E., Moser, C., Olafson, J., Palmer, M.R., Rudinicki, M.D. 1994. Hydrothermal activity on the Reykjanes Ridge: the Steinaho II Vent-field at 63_060N. *Earth Planet Sci Lett* 121:647-654.
- Giambalvo, E.R., Fisher, A.T., Martin, J.T., Darty, L., Lowell, R.P. 2000. Origin of elevated sediment permeability in a hydrothermal seepage zone. eastern flank of the Juan de Fuca Ridge. and implications for transport of fluid and heat. *J. Geophys. Res* 105:913-928.
- Hamza. V.M. 1967. The relationship of heat flow with geologic age. Internal Report. National Geophysical Res. Institute. Hyderabad (India).
- Hamza, V.M. 1979. Variation of continental mantle heat flow with age: Possibility of discriminating between thermal models of the lithosphere, *Pure and Applied Geophysics*, vol. 117, pp. 65 - 74.
- Hamza, V.M. 2013. Global Heat Flow without invoking 'Kelvin Paradox', *Frontiers in Geosciences*, Volume 1, No.1, PP. 11-20.
- Hamza, V.M., Cardoso, R.R., Alexandrino, C.H. 2010. A magma accretion model for the formation of oceanic lithosphere: Implications for global heat loss, *International Journal of Geophysics*, pp. 1-16.
- Hamza V.M., Cardoso R.R., Ponte Neto C.F. 2008a. Spherical Harmonic Analysis of Earth's Conductive Heat Flow. *International Journal of Earth Sciences*, 97, 205-226.
- Hamza V.M., Cardoso R.R., Ponte Neto C.F. 2008b. Reply to comments by Henry N. Pollack and David S. Chapman on "Spherical harmonic analysis of Earth's conductive heat flow". *International Journal of Earth Sciences*, 97, 233-239.
- Hamza, V.M., Verma, R.K. 1969. Relationship of heat flow with the age of basement rocks, *Bull. Volcan.*, 33, 123-152.
- Haymon, R.M., Fornari, D.J., Edwards, M.H., Carbotte, S., Wright, D., Macdonald, K.C. 1991. Hydrothermal vent distribution along the East Pacific Rise crest (9o09'-54' N) and its relationship to magmatic and tectonic processes on fast-spreading mid-ocean ridges. *Earth Planet. Sci. Lett.*, 104:513-534.
- Hofmeister, A.M., Criss, R.E. 2005. Earth's heat flux revised and linked to chemistry, *Tectonophysics*, vol. 395, pp. 159-177.
- Hofmeister, A.M.; Criss, R.E. 2006. Comment on "Estimates of heat flow from Cenozoic sea floor using global depth and age data", by M. Wei and D. Sandwell", *Tectonophysics*, vol. 428, pp. 95-100.
- Hofmeister, A.M., Criss, R.E. 2008. Model or measurements? A discussion of the key issue in Chapman and Pollack's critique of Hamza et al.'s re-evaluation of oceanic heat flux and the global power, *International Journal of Earth Sciences*, vol. 97, pp. 239-243.
- INGEOMINAS. 2009. Mapa geotérmico de Colombia, Instituto De Investigación E Información Geocientífica, Minero Ambiental Y Nuclear, Exploración Y Evaluación De Recursos Geotérmicos. República De Colombia, Ministerio De Minas Y Energía, Bogotá, Colombia.
- Jessop, A. M., Hobart, M. A., Sclater, J. G. 1976. The World Heat Flow Data Collection - 1975, *Geothermal Series 5*, Earth Phys. Branch, Ottawa, 125 p.
- Lee W.H.K. 1963. Heat flow data analysis. *Reviews of Geophysics*. 1:449-479.
- Lee W.H.K., Uyeda S. 1965. Review of heat flow data. In: Lee W.H.K (Eds) *Terrestrial heat flow*. Geophysical monograph series 8. AGU. Washington. pp 87-100.
- McKenzie, D.P. 1967. Some remarks on heat flow and gravity anomalies. *J. Geophys. Res.*, 72, 6261 - 6273.
- Mooney. W.D., Laske, G., Masters T.G. 1998. CRUST 5.1: A global crustal model at 5° × 5°. *J. Geophys. Res*. V. 103. No. B1. 727-747. 1998.
- Muller. R.D., Roest. W.R., Royer. J., Gahagan. L.M., Sclater J.G. 1997. Digital isochrones of the world's ocean floor. *J. Geophys. Res*. 102. B2. 3211-3214.

Parsons, B., Sclater, J. G. 1977. An analysis of the variation of ocean floor bathymetry and heat flow with age, *J. Geophysics. Res.*, 82, 803-827.

Pollack H.N., Hurter S.J., Johnson J.R. 1993. Heat flow from the earth's interior: analysis of the global data set. *Rev. Geophys.*, 31, 267-280.

Polyak B.G., Smirnov Y.A. 1968. Relationship between terrestrial heat flow and tectonics of continents. *Geotectonics*, 4, 205-213 (Eng. Transl.).

Sclater, J.G, Jaupart, C, Galson, D. 1980. The heat flow through oceanic and continental crust and heat loss of the Earth. *Rev Geophys.* 18:269-311.

Stein, C., Stein, S. 1992. A model for the global variation in oceanic depth and heat flow with lithospheric age. *Nature* 359:123-129.

Vieira, F.P., Cardoso, R.R., Hamza, V.M. 2010. Global Heat Loss: New Estimates Using Digital Geophysical Maps and GIS Techniques. Proceedings of the IV Brazilian Symposium on Geophysics, 14 - 17 November, Brasília.

Vieira, F.P., Hamza, V.M. 2011. Global Heat Flow: Comparative analysis based on experimental data and theoretical values. Proceedings of Twelfth International Congress of the Brazilian Geophysical Society, 1-6.

Vieira, F. P., Cardoso, R.R., Hamza, V.M. 2010. Global Distribution of Mantle Heat Flow. In: The Meeting of the Americas, AGU, Foz do Iguaçu - PR (Brazil).

Williams, D.L., Von Herzen, R.P., Sclater, J.G., Anderson, R.N. 1974. The Galapagos spreading center: lithospheric cooling and hydrothermal circulation. *Geophys. J R Astron. Soc.* 38:587-608.

Appendix – Finite Half-Space Model

Analytical expressions for variation of temperature (T) with time (t) and depth (z) in such a boundary layer may be obtained as solution to the one-dimensional heat conduction equation:

$$\frac{\partial T}{\partial t} = \kappa_{mod} \frac{\partial^2 T}{\partial z^2} \quad (A1)$$

where κ_{mod} is the modified thermal diffusivity that takes into consideration the effect of latent heat. If the wavelength of the problem addressed in Eq. (A1) is assumed to be large ($z \rightarrow \infty$) its solution may be expressed in terms of the error function (erf) as (Carslaw and Jaeger, 1959):

$$\frac{T(z, t) - T_0}{T_m - T_0} = \text{erf}\left(\frac{z}{2\sqrt{\kappa t}}\right) \quad (A2)$$

Introducing the dimensionless variables:

$$\theta = \frac{T_m - T}{T_m - T_0} \quad \text{and} \quad \eta = \frac{z}{\sqrt{4\kappa_{mod} t}} \quad (A3)$$

equation (A1) may be written as:

$$-\eta \frac{\partial \theta}{\partial \eta} = \frac{1}{2} \frac{d^2 \theta}{d \eta^2} \quad (A4)$$

The introduction of the similarity variable reduces the partial differential equation (A1) to an ordinary differential

equation (A4) in the variable η . This is appropriate as long as the similarity solution satisfies the required boundary conditions.

The boundary conditions ($T = T_0$ at $z = 0$ and $T = T_m$ at $z = a$) when expressed in terms of the similarity variables become:

$$\theta = 1 \text{ at } \eta = 0 \text{ and } \theta = 0 \text{ at } \eta = a/\sqrt{4\kappa_{mod} t} \quad (A5)$$

where “a” is the thickness of the oceanic lithosphere at large distances from the ridge axis. Following standard procedures (see for example, Turcotte and Schubert, 1967; Ozisik, 1980) the solution of equation (A3) is:

$$\theta = C_1 \int_0^\eta e^{-\eta'^2} d\eta' + 1 \quad (A6)$$

where η' is a dummy variable of integration and the boundary condition $\theta(0) = 1$ is used to evaluate the second constant of integration. To satisfy the second boundary condition:

$$\theta(a/\sqrt{4\kappa_{mod} t}) = 0$$

it is necessary to have

$$0 = C_1 \int_0^{a/\sqrt{4\kappa_{mod} t}} e^{-\eta'^2} d\eta' + 1 \quad (A7)$$

The definite integral is:

$$\int_0^{a/\sqrt{4\kappa_{mod} t}} e^{-\eta'^2} d\eta' = \frac{\sqrt{\pi}}{2} \text{erf}\left(\frac{a}{\sqrt{4\kappa_{mod} t}}\right) \quad (A8)$$

Thus, the constant C1 is:

$$C_1 = \frac{-2}{\sqrt{\pi}} \frac{1}{\text{erf}\left(a/\sqrt{4\kappa_{mod} t}\right)} \quad (A9)$$

Substitution of C1 into (A5) and rearranging the terms gives:

$$\theta = 1 - \frac{\text{erf}\left(z/\sqrt{4\kappa_{mod} t}\right)}{\text{erf}\left(a/\sqrt{4\kappa_{mod} t}\right)} \quad (A10)$$

Substitution of (A2) into (A9) gives:

$$\frac{T - T_0}{T_m - T_0} = \frac{\text{erf}\left(z/\sqrt{4\kappa_{mod} t}\right)}{\text{erf}\left(a/\sqrt{4\kappa_{mod} t}\right)} \quad (A11)$$

Note that for small values of t and z the right-hand side of Eq. (A11) is nearly identical to that of the fundamental solution for temperatures in the HSC model. On the other hand, for values of z equal to a , the right-hand side of Eq. (A11) approaches unity, which is the limiting condition employed in the Plate model.